



HAL
open science

Identification of incommensurability in L-leucine: can lattice instabilities be considered as general phenomena in hydrophobic amino acids?

Yannick Guinet, Laurent Paccou, Florence Danede, Patrick Derollez, Alain Hedoux

► To cite this version:

Yannick Guinet, Laurent Paccou, Florence Danede, Patrick Derollez, Alain Hedoux. Identification of incommensurability in L-leucine: can lattice instabilities be considered as general phenomena in hydrophobic amino acids?. *Physical Chemistry Chemical Physics*, 2022, *Physical Chemistry Chemical Physics*, 24 (44), pp.27023-27030. 10.1039/d2cp00989g . hal-03871324

HAL Id: hal-03871324

<https://hal.univ-lille.fr/hal-03871324v1>

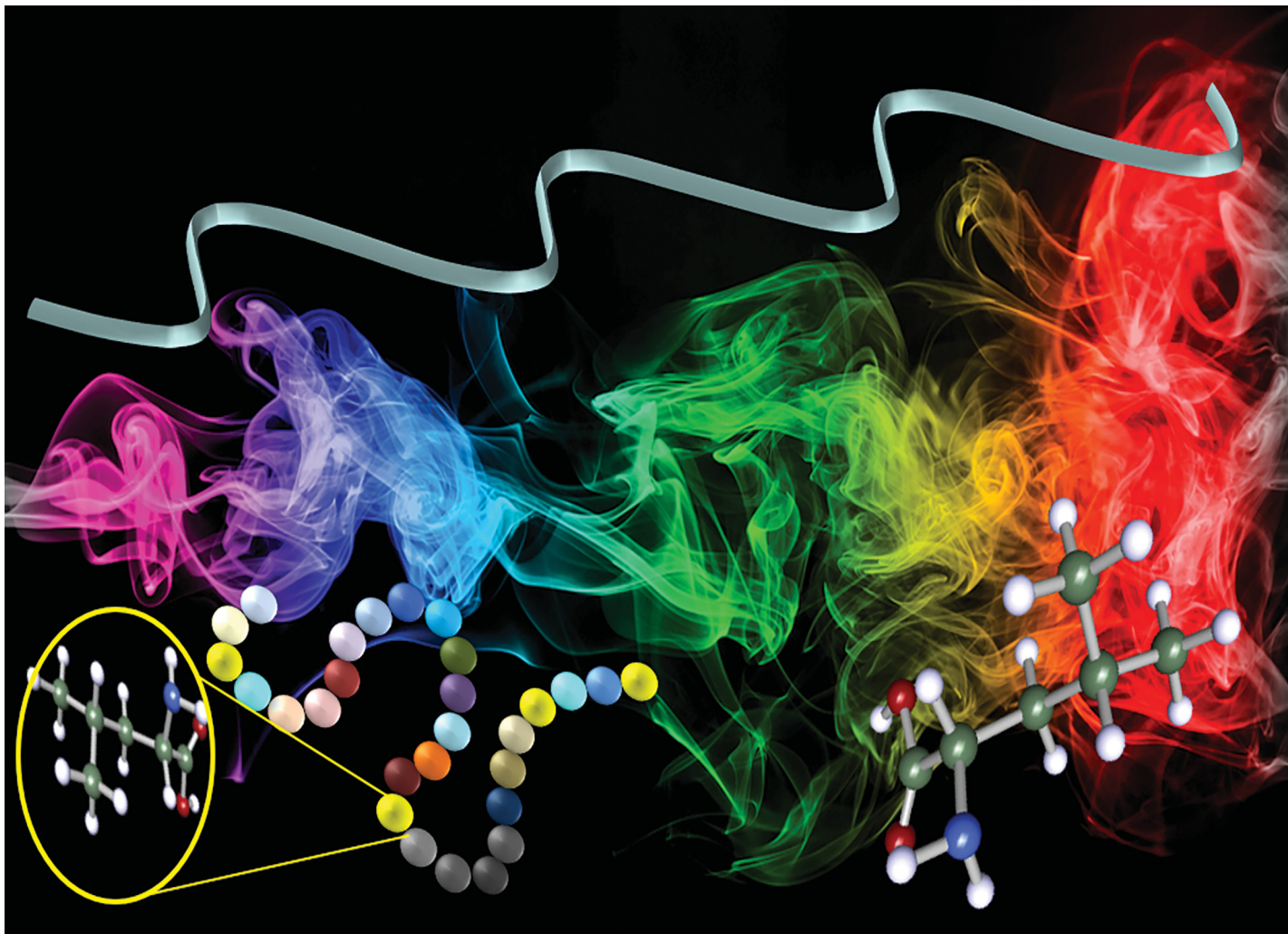
Submitted on 25 Nov 2022

HAL is a multi-disciplinary open access archive for the deposit and dissemination of scientific research documents, whether they are published or not. The documents may come from teaching and research institutions in France or abroad, or from public or private research centers.

L'archive ouverte pluridisciplinaire **HAL**, est destinée au dépôt et à la diffusion de documents scientifiques de niveau recherche, publiés ou non, émanant des établissements d'enseignement et de recherche français ou étrangers, des laboratoires publics ou privés.



Distributed under a Creative Commons Attribution 4.0 International License

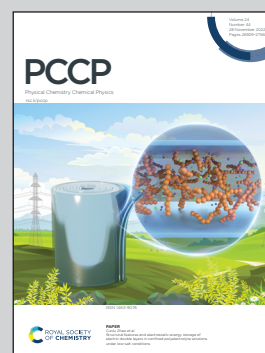


**Showcasing research from the group of Professor
Alain Hédoux in UMET, University of Lille**

Identification of incommensurability in L-leucine: can
lattice instabilities be considered as general phenomena
in hydrophobic amino acids?

Fundamental research developed in the Hédoux group focusses
on the structure and dynamics of molecular glass-forming
materials with applications in the pharmaceutical area.
A major concern is the control and manipulation of the
material physical state for improving bioavailability and
stability, from understanding phase transition mechanisms.
Amino acids are widely used as excipients in freeze-dried,
spray-dried, co-amorphous formulations, and as building
blocks of proteins. Predicting their dynamical instabilities
is a crucial issue for stabilizing active molecules and
biomolecules.

As featured in:




See Alain Hédoux *et al.*,
Phys. Chem. Chem. Phys.,
2022, **24**, 27023.



Cite this: *Phys. Chem. Chem. Phys.*, 2022, 24, 27023

Identification of incommensurability in L-leucine: can lattice instabilities be considered as general phenomena in hydrophobic amino acids?†

Yannick Guinet, Laurent Paccou, Florence Danède, Patrick Derollez and Alain Hédoux *

L-Leucine is an essential amino acid which has been focusing a lot of investigations on its phase transition sequence for more than fifty years. Combining Raman spectroscopy and X-ray diffraction experiments provides a new interpretation of the second order phase transition extending between 270 and 360 K as a displacive incommensurate-normal phase transition. A soft mode was clearly detected from low-frequency Raman investigations which exhibits the temperature dependence $(A \cdot (T_C - T)^{1/2})$ typical of the temperature behavior of the amplitudon, an excitation specific to incommensurate phases. Simultaneously to the softening of the amplitudon, several very weakly intense X-ray reflections vanish upon heating at 360 K, and thereby are interpreted as satellite reflections. This incommensurability was described as resulting from the freezing of thermally activated hydrophobic side-chain rotations upon cooling in disordered orientations. Raman investigations were also performed on the isomeric amino acid L-norleucine previously identified as undergoing a normal-incommensurate phase transition around 200 K. Comparison of both studies suggests that the temperature behavior of thermally activated local motions generates lattice instabilities. Loss of periodicity can result from the freezing of rotations of molecular moieties in disordered orientations, or from the enhancement of anharmonicity of these rotations. This could be a general phenomenon in hydrophobic amino acids with direct consequences on their applications in the life science area.

Received 28th February 2022,
Accepted 26th July 2022

DOI: 10.1039/d2cp00989g

rsc.li/pccp

1. Introduction

L-Leucine ($C_6H_{13}NO_2$, LEU) is an essential amino acid, used in the biosynthesis of proteins. In addition to the α -amino group, it contains an α -carboxylic acid group and a side chain isobutyl group (see Fig. S1, ESI†) which can reorientate¹ under certain conditions, and can be reminiscent within the protein structure. It is now well recognized that protein function is closely connected to the protein dynamics.^{2–6} However, local side-chain motions are also considered as a possible source of protein unfolding.⁷ Beyond the impact of side chain motions on protein flexibility, this type of thermally activated motion can also

impact the physical state of inhaled powder formulations obtained by the spray-drying technology in which LEU is widely used as an excipient.^{8–10} Several previous studies have revealed successive phase transitions in LEU in a wide temperature range (from 70 K to 370 K) using various techniques.¹¹ A high-temperature phase transition around 353 K was reported in several papers^{12,13} without a clear description of the nature of the transition. However the structural description determined at 120 K¹⁴ is identical to that determined at room temperature,^{15,16} and no change in the spatial group was reported until now. In this paper, we first demonstrate that this transition is a normal-incommensurate phase transition associated with thermally activated disorder of terminal side-chain atoms, from Raman spectroscopy, differential scanning microcalorimetry (DSC) and X-ray powder diffraction (XRPD) investigations. The investigations carried out on L-leucine were compared with those performed on L-norleucine, previously identified as undergoing an ordering process upon cooling *via* modulated (incommensurate and commensurate) structures. Norleucine (Nle) is a linear isomer of leucine and is also a chiral molecule as leucine and most of the α amino acids are. The chemical structure of norleucine is compared with that of leucine in Fig. S1 in the ESI.† Norleucine

University of Lille, CNRS, INRAE, Centrale Lille, UMR 8207 - UMET - Unité Matériaux et Transformations, F-59000 Lille, France.

E-mail: alain.hedoux@univ-lille.fr

† Electronic supplementary information (ESI) available: Structural descriptions of L-leucine and L-norleucine (Fig. S1); description of the fitting procedure of the low-frequency Raman spectrum (Fig. S2); description of the fitting procedure of the high-frequency Raman spectrum in the C–H stretching mode region (Fig. S3); description of the refinements of the X-ray powder diffraction patterns at 293 K and 373 K (Fig. S4); and results of the refinements of the X-ray powder diffraction data (Table S1). See DOI: <https://doi.org/10.1039/d2cp00989g>



is nearly isosteric with methionine, although it doesn't contain a sulfur atom¹⁷ which is considered as partly responsible for a high side-chain flexibility. Low-frequency Raman investigations have revealed a very progressive disordering upon heating L-methionine (L-Met) from 170 K up to 420 K, correlated with the partial softening of lattice modes. Consequently, similar investigations were carried out on leucine and norleucine and were compared with those performed on methionine in order to better understand the origin of the phase transition sequence in hydrophobic amino acids.

2. Experimental

2.1. Materials

L-Leucine (C₆H₁₃NO₂, L-LEU, purity > 98%) and L-norleucine (C₆H₁₃NO₂, L-Nle, purity > 98%) were purchased from Sigma-Aldrich and used as received without additional purification.

2.2. Methods

Micro calorimetry experiments were carried out using a very sensitive microcalorimeter (microDSC III, Setaram) using the 3-dimensional sensor technology. A typical mass of 400 mg of L-leucine powder was input in one furnace, and a similar mass of alumina was input in the second furnace. Both furnaces were hermetically closed. Only 1 K min⁻¹ heating runs from 260 K to 420 K were analyzed.

Low-frequency Raman spectra were collected using a high-resolution Raman XY-Dilor spectrometer to analyze the non-polarized back-scattered light. The spectrometer is composed of a double monochromator comprising four mirrors characterized by a focal length of 800 mm and a spectrograph. The choice of experimental conditions (incident radiation, entrance and exit slit width opened at 200 μm) gives a spectral resolution of about 1 cm⁻¹ in the 5–250 cm⁻¹ region, with the high rejection of excitation light (the 660 nm line of a solid diode laser) making it possible to detect Raman signal from 5 cm⁻¹. The spectrometer is equipped with a liquid nitrogen cooled charge coupled device detector. The high sensitivity of the detector and the large analyzed scattered volume (~0.5 cm³) allow us to record low-wavenumber Raman spectra in the 5–250 cm⁻¹ range in 120 seconds. Powder samples were loaded in spherical pyrex cells that were hermetically sealed. The temperature of the sample was regulated using an Oxford nitrogen flux device that keeps temperature fluctuations within 0.1 °C. Spectra were collected during 1 K min⁻¹ heating ramps with an acquisition time of 60 seconds allowing the collection of 1 spectrum per degree.

High-frequency Raman investigations were performed using an InVia Renishaw Raman microscope in the 2800–4000 cm⁻¹ region equipped with a solid diode laser emitting the 514.5 nm radiation. An achromatic lens was used for analyzing a large volume of the powder sample. The sample temperature was controlled by placing the sample in a THMS 600 Linkam temperature device. Spectra were collected during 1 K min⁻¹ heating ramps in the same conditions as performed in the low-frequency region.

X-Ray diffraction was performed on as-received LEU powder using a Panalytical X'pert PRO MPD diffractometer. The Debye-Scherrer geometry was used, operating with the CuKα_{1,2} radiation selected by a hybrid monochromator. The Lindemann glass capillary (∅ = 0.7 mm) mounted at the center of the goniometer circle was rotating around the horizontal axis during the data collection in order to ensure the proper averaging over the individual crystallites. LEU powder was heated in a Hubert HTC 9634 furnace composed of a Kapton window giving a diffuse intensity to the diffraction pattern below 2θ = 7°. Consequently, the most intense Bragg peak of the diffraction pattern (detected around 2θ ~ 6°) was omitted in the refinement procedures. The X-ray diffraction patterns collected at room temperature and at 373 K were refined using the “profile matching” option called Le Bail refinement¹⁸ of the Fullprof program¹⁹ from cell parameters given by Coll *et al.*²⁰

3. Results and discussion

3.1. Raman spectroscopy

Low-frequency Raman (LFR) investigations were carried out on L-LEU in the temperature range of 220–360 K covering the broad 2nd order transition.¹² LEU was first cooled down to 220 K, in order to completely analyze the extended transformation observed by calorimetry. LFR spectra collected continuously upon heating at 1 K min⁻¹ from 220 K to 370 K are plotted by step of 1 K from 220 to 350 K in Fig. 1a, and by step of 5 K in Fig. 1b using a logarithm ω-scale for better deciphering the low intensity phenomenon in the very low-frequency region. Fig. 1a highlights a clear contrast between phonon peaks detected below 60 cm⁻¹ that shift towards the low-frequencies and other lattice modes which are almost temperature independent. At the lower frequencies, a broad peak is detected tailing a sharp band around 30 cm⁻¹. This low-frequency band exhibits significant broadening and shifts towards the low frequencies upon heating, accompanied by the broadening of the quasi-elastic scattering. The overdamped behavior of this band is typical of that of a soft mode observed in various normal – incommensurate (N-INC) phase transitions.²¹

Low-frequency Raman spectra collected upon heating L-Nle are plotted in Fig. 2. Investigations were carried out with similar conditions ($\dot{T} = 1 \text{ K min}^{-1}$) as for L-LEU, but over a wider temperature range (120–450 K) since several phase transitions were previously observed in this temperature range.²² In the low-temperature range plotted in Fig. 2b, a sharp and weak intense band is clearly detected in the very low-frequency region below 25 cm⁻¹, localized by an arrow at 120 K in Fig. 2a. This band is almost temperature independent up to 150 K and broadens by shifting towards the lower frequencies upon further heating, giving a significant contribution to the quasielastic scattering (localized by an arrow) at 180 K in Fig. 2a. It is the typical temperature behavior of a soft mode, which can be associated with the N-INC phase transition previously observed around 200 K.²² At higher temperatures, Fig. 2b clearly shows that the disordering progressively continues upon heating *via* the



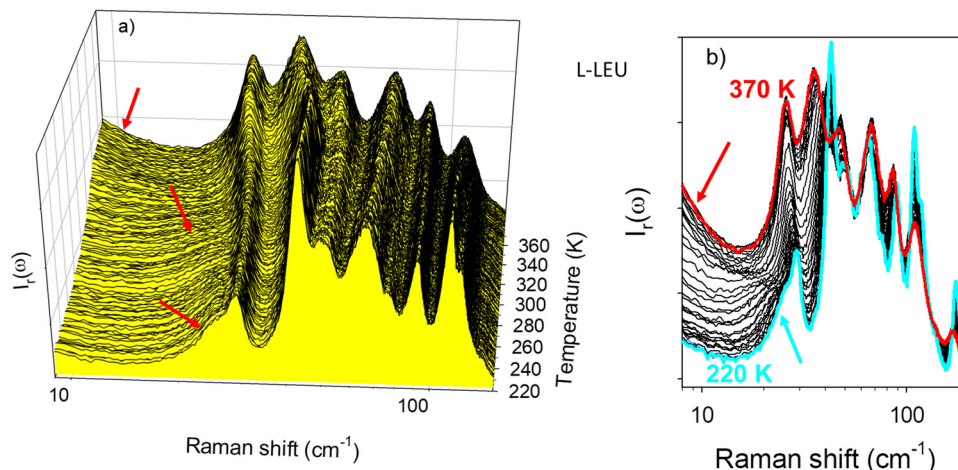


Fig. 1 Low-frequency Raman spectra of L-LEU collected upon heating from 220 K at 1 K min^{-1} , (a) plotted by step of 1 K, (b) plotted by step of 5 K, arrows are used to show the temperature behavior of the soft mode.

observation of the broadening and the downshift of the phonon peaks below 50 cm^{-1} , giving a pronounced contribution to the quasielastic scattering. At temperatures above 400 K, no phonon peak can be longer detected, the spectrum resembling the vibrational density of states (VDOS) of a very disordered state, as recently observed in L-methionine.²³

Phonon frequencies of lattice modes were determined using the fitting procedure shown in the Fig. S2 (ESI[†]) for L-LEU. The frequency temperature dependences of the low-frequency phonon peaks detected below 60 cm^{-1} are plotted in Fig. 3a and b for L-LEU and L-Nle, respectively.

The softening of the lowest frequency phonon is clearly observed in both compounds. Approaching the phase transition upon heating, the soft modes become a tail of the Rayleigh wing and the fit parameters of the bands (intensity, frequency and width) cannot be satisfactorily defined. Upon further heating above the phase transition, the soft modes are merging into the quasielastic scattering reflecting the local dynamics in L-LEU and L-Nle. At higher frequencies, Fig. 3 highlights a strong contrast between the temperature dependences of lattice modes in L-LEU

and L-Nle, which can be also observed by comparing Fig. 1 and 2. Indeed, Fig. 3b is dominated by the strong downshift of lattice modes upon heating merging into a broad low-frequency hump observed in Fig. 2b as mimicking a VDOS of a disordered state. By contrast, lattice modes in L-LEU exhibit slighter downshifts upon heating reflecting a less marked anharmonic character than in L-Nle, probably resulting from a lesser degree of side-chain flexibility.

The very low-frequency region of Raman spectra in molecular materials is characterized by the overlapping of vibrational and relaxational contributions. The two types of motions can be separated by the fitting procedure described in Fig. S3 in the ESI[†] regardless of the degree of disorder. The relaxational contribution also called quasielastic scattering is associated with fast local motions that are thermally activated, generally corresponding to large amplitude rotations of groups of atoms within the molecule, and is well described by a Lorentzian peak centered at $\omega = 0$. The temperature dependence of the quasielastic intensity is very suited for detecting order-disorder transformations. The quasielastic intensity (I_{QES}) was obtained

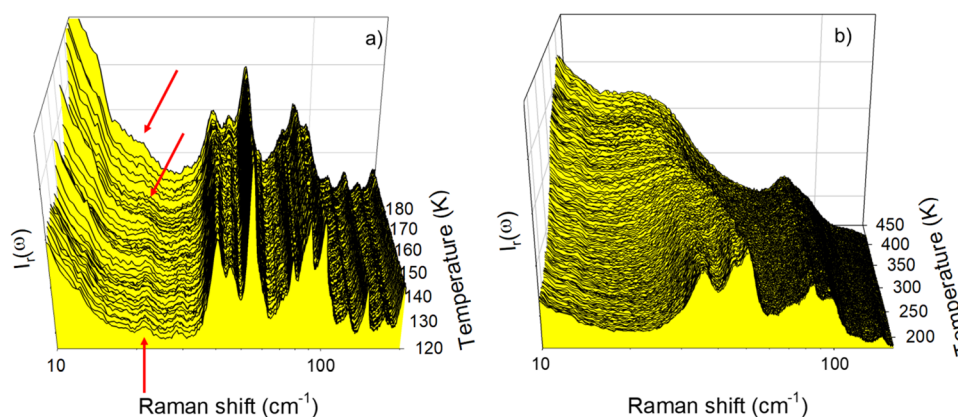


Fig. 2 Low-frequency Raman spectra of L-Nle collected upon heating from 120 K at 1 K min^{-1} plotted by step of 1 K (a) in the 120–180 K temperature range, (b) in the 180–450 K temperature range; arrows show the soft mode.



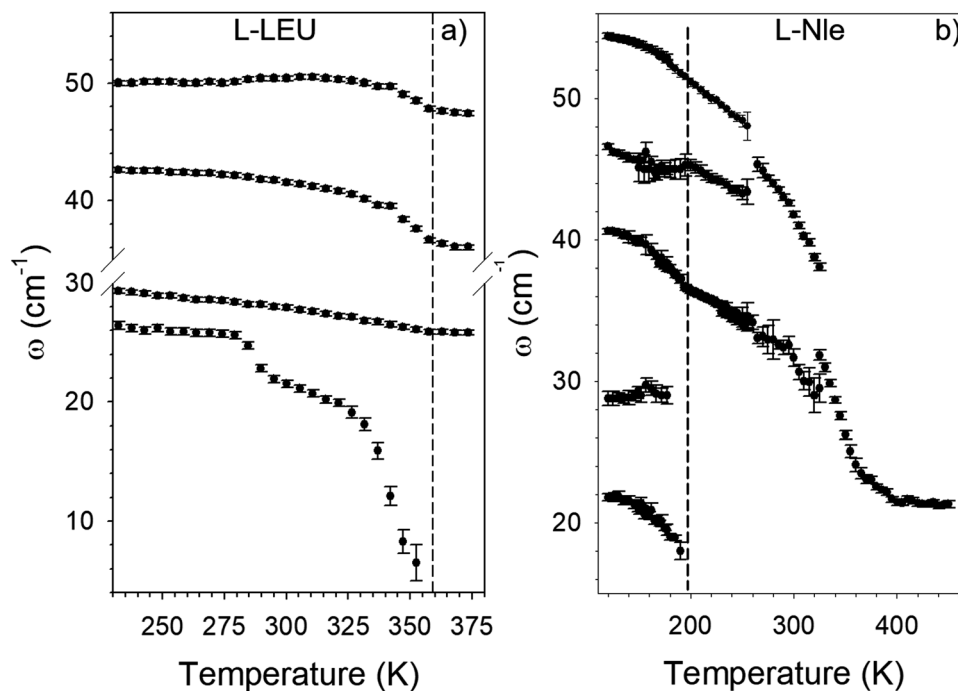


Fig. 3 Temperature dependences of lattice modes frequencies (a) in L-leucine, (b) in L-norleucine; dashed lines indicate the incommensurate – normal transition in both amino acids.

by integrating the Lorentzian peak after renormalization by the intensity of lattice modes in the 70–150 cm^{-1} region, not affected by the relaxational contribution. The $I_{\text{QES}}(T)$ curve is plotted in Fig. 4a for each amino acid. It can be observed in Fig. 4 that both $I_{\text{QES}}(T)$ curves have an exponential behavior in the same temperature range delimited by dashed vertical lines, and a linear behavior outside. This temperature behavior can be fitted between 260 and 360 K, using an Arrhenius relation $Ae^{-E_a/RT}$ for determining the activation energy E_a . Fitting procedures lead to $E_a = 11.6 \pm 0.2 \text{ kJ mol}^{-1}$ for L-LEU and $E_a = 8.3 \pm 0.8 \text{ kJ mol}^{-1}$ for L-Nle. A similar $I_{\text{QES}}(T)$ -curve shape was obtained in L-methionine in the same limited T-range from 260 K up to 360 K, corresponding to the disordering process characterized by

a broad endotherm.²³ Consequently, the heat flow trace obtained upon heating was compared with $I_{\text{QES}}(T)$ for L-LEU. Fig. 4b reveals a spread transformation extending over 80 K, in accordance with the previous investigations.¹² The heat flow trace is typical of a broad second-order behavior, with a long tail on the low-temperature side, which can be considered as the calorimetric signature of a normal (N)–incommensurate (INC) transition observed in L-Nle²² and in A_2BX_4 materials.²⁴ In incommensurate crystals, the displacive N–INC phase transition is induced by the condensation of a soft lattice vibrational mode.^{21,25–27} The displacive nature of the phase transition is characterized by the temperature dependence of the order parameter directly related to the amplitude of small atomic displacements.²⁸ Fig. 4b shows that

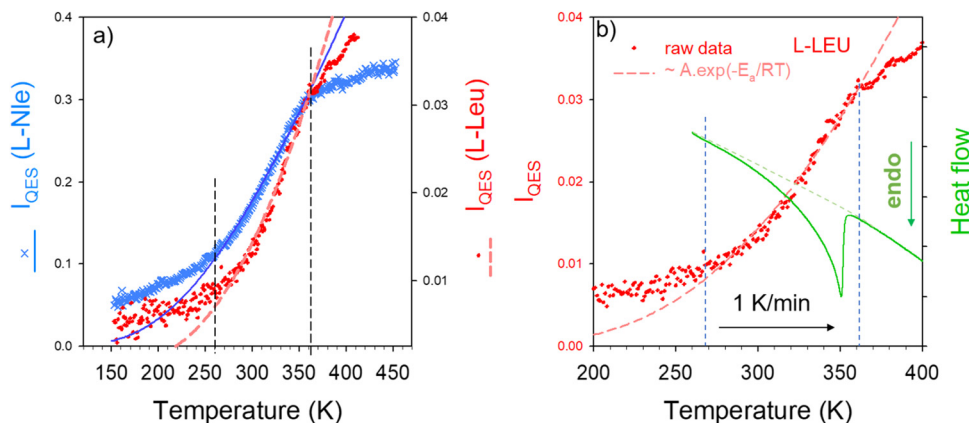


Fig. 4 Temperature dependence of the quasielastic intensity (I_{QES}); (a) comparison of $I_{\text{QES}}(T)$ in L-LEU and L-Nle, (b) comparison of $I_{\text{QES}}(T)$ with the heat flow trace in L-LEU.



the exponential behavior of $I_{QES}(T)$ is covering the temperature range in which both the broad endotherm and the softening of the lattice mode were observed. It is worth noting that DSC experiments performed on L-Nle²² have also revealed an extended transformation in the 250–370 K temperature range, above the N-INC phase transition at 210 K.

The temperature dependence of the quasielastic intensity is considered as proportional to that of mean square displacements $\langle u^2 \rangle$ of rigid groups of atoms including local protein side-chain motions.²⁹ This indicates that there is a direct connection between the extended phase transition and the thermal activation of hydrophobic side-chain motions.

High-frequency Raman investigations were performed in order to analyze C–H stretching vibrations since several studies have revealed the involvement of local motions of CH₃ groups in the phase transitions at low-temperatures (below 275 K) in L-LEU¹¹ and other amino acids.^{23,30} These considerations have motivated the analysis of the high-frequency spectrum in the 2500–3200 cm⁻¹ region that is usually dominated by the C–H stretching vibrations. This analysis was performed using the InVia Renishaw spectrometer in the 270–390 K temperature range. Spectra are plotted in Fig. 5a by step of 5 K. The C–H stretching region is generally temperature independent³¹ except on either side of a phase transition. By contrast to this behavior, Fig. 5a clearly shows a continue temperature dependence of the C–H stretching spectrum between 270 K and 360 K. The two first Raman bands located at 2869 and 2901 cm⁻¹ exhibit two opposite temperature dependences, schematized by the arrows in Fig. 5a. The temperature dependences of these bands were carefully analyzed using a fitting procedure described in Fig. S4 in the ESI.† The frequency temperature dependences of these bands are plotted in Fig. 5b.

The lowest frequency band (~ 2869 cm⁻¹) is characterized by a weakly positive temperature dependence of its position ($d\omega/dT > 0$) considered as the signature of H-bonding molecular associations.³¹ This band can be assigned to the

stretching of the C–H group interacting with the oxygen atom of the neighboring molecule in agreement with X-ray diffraction data.¹⁴ Around 2900 cm⁻¹ the frequency of the Raman band exhibits an unusual non-linear negative temperature behavior, as previously observed in L-methionine,²³ much larger than that of the 2869 cm⁻¹ band. Both bands become temperature independent above 360 K.

The large and non-linear temperature dependence of the 2900 cm⁻¹ band observed both in Fig. 5a and b is undoubtedly related to the reorientational motions of CH₃ groups, given that this band was assigned to C–H stretching vibrations in CH₃ groups.¹³ The unusual temperature dependence of the 2900 cm⁻¹ band for a C–H stretch was compared with the temperature dependence of the soft phonon frequency in Fig. 6. Interestingly, the temperature dependences of C–H stretch and soft mode are superimposed, indicating a close relationship between the lattice instability and reorientations of CH₃ groups. Given that the fitting procedure of the soft mode fails approaching T_c , the temperature dependence of the soft mode (SM) frequency will be considered as similar to that of the 2900 cm⁻¹ band. The temperature dependence of C–H stretching frequency was fitted with the function $A(T_c - T)^n$ in the whole 270–360 K temperature range. Fig. 6 shows that the temperature dependences of both low- and high-frequency bands are correctly described by the function $(T_c - T)^{1/2}$, with $T_c = 360$ K and $n = 0.51 \pm 0.04$. This is the typical temperature dependence of the amplitude mode, the so-called amplitudon, in incommensurate modulated phases.²¹ Fig. 6 shows that the low-frequency mode is typical of the lattice dynamics of modulated phases, and the C–H stretching band frequency has a clear order parameter behavior for a second-order phase transition. This indicates that the normal – incommensurate phase transition is driven by the freezing of reorientational motions of CH₃ groups in disordered orientations upon cooling.

High-frequency Raman investigations were also performed in the C–H stretching regions of L-Nle. Spectra collected upon

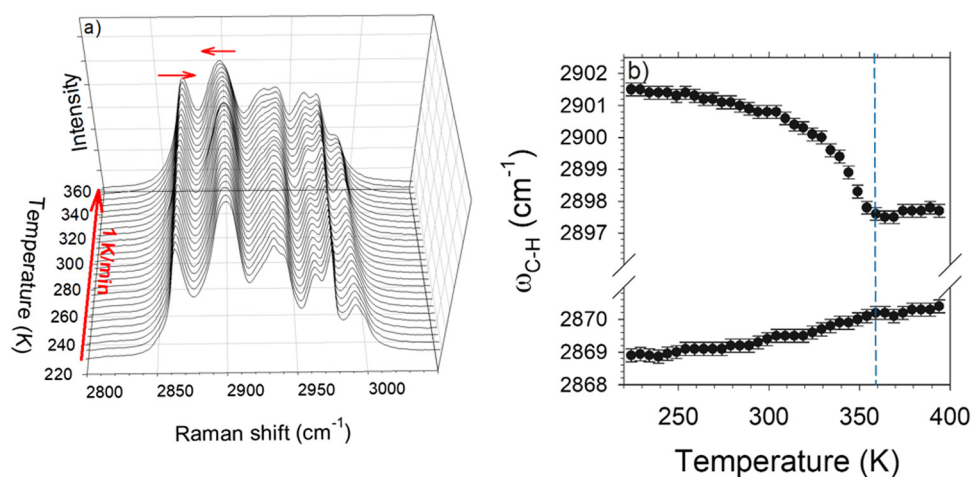


Fig. 5 Temperature dependence of C–H stretching vibrations. (a) Plot of spectra collected during a heating ramp from 220 K at 1 K min⁻¹. The horizontal arrows show the opposite temperature dependence of the lowest frequency bands in the C–H stretching region. (b) Temperature dependence of the frequencies of the C–H stretching bands schematically displayed by the arrows in the plot of spectra.



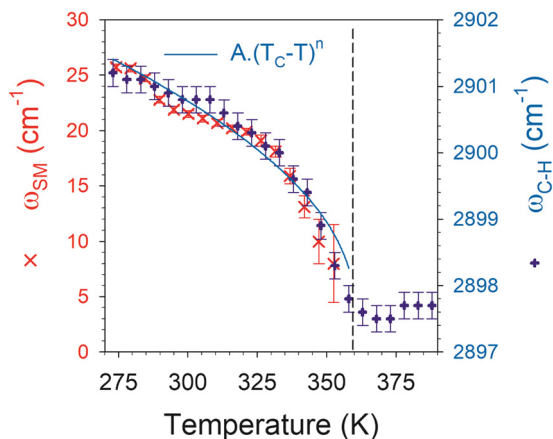


Fig. 6 Combination of low- and high-frequency Raman analyses. Comparison of the temperature dependence of the C–H stretching band frequency at 2900 cm^{-1} with that of the soft mode; symbols result from fitting procedures of lattice modes and C–H stretching spectra, and the line corresponds to the fitting procedure of C–H stretching frequencies with the function $A \cdot (T_C - T)^n$ with $T_C = 360\text{ K}$. The fitting procedure is converging towards the parameters: $A = 0.39 \pm 0.06$ and $n = 0.51 \pm 0.04$ ($R = 0.977$).

heating L-Nle at 1 K min^{-1} from 120 K are plotted in Fig. 7a. Significant spectral modifications corresponding to the broadening and shifts of Raman bands can be easily detected. Some of them can be observed by plotting the frequency temperature dependences of C–H stretching bands in the $2930\text{--}2980\text{ cm}^{-1}$ region. The frequencies were obtained by fitting the whole C–H stretching region plotted in Fig. 7a, as performed for L-LEU. Significant downshifts are observed in the very low-temperature range ($<170\text{ K}$) and above 250 K , *i.e.* in the same temperature range as observed in L-LEU. Additionally, the downshifts of 2 bands detected above 250 K in L-Nle also correspond to a broad endothermic transformation²² but not corresponding to the

INC–N phase transition. The simultaneous analysis of Fig. 3b, 4a and 7b shows that the exponential temperature behavior of I_{QES} coincides with the drastic downshift of two C–H stretching bands and the large but incomplete softening of the 50 cm^{-1} lattice mode. This is the indication that thermally activated motions of CH_n groups are responsible for lattice instabilities in L-Nle. The comparison of Fig. 1 and 2 shows that the degree of disorder is significantly higher in L-Nle than in L-LEU. The consequence is a very progressive ordering of CH_n groups in L-Nle over a wide temperature range characterized by the freezing in disordered CH_n orientations at lower temperatures than in L-LEU.

4. Powder X-ray diffraction

A modulated INC phase is usually characterized by the presence of satellite lines in the X-ray diffraction pattern, which have weaker intensities than Bragg peaks, as observed in N-Nle,²² vanishing at the INC–N transition. In order to observe these satellite peaks, the X-ray powder diffraction (XRPD) pattern was analyzed between the room temperature and 470 K . XRPD diagrams are plotted in Fig. 8a. This figure confirms the presence of satellite lines *via* the detection of several peaks (marked by arrows in Fig. 8a) characterized by a low intensity vanishing at $T_C \sim 360\text{ K}$. The temperature dependence of the integrated intensity of the most intense satellite reflection is plotted in Fig. 8b. This temperature behavior is typical of satellite reflections observed in other incommensurate phases³² and is also well described by the function $(T_C - T)^n$. The XRPD pattern was analyzed at $T = 293\text{ K}$ and $T = 373\text{ K}$, *i.e.* on both sides of the temperature of INC–N transition ($\sim 360\text{ K}$). The best reliability factors of the Le Bail refinement procedures of the XRPD patterns (described in Fig. S4, ESI†) are obtained with the same monoclinic cell parameters given in the

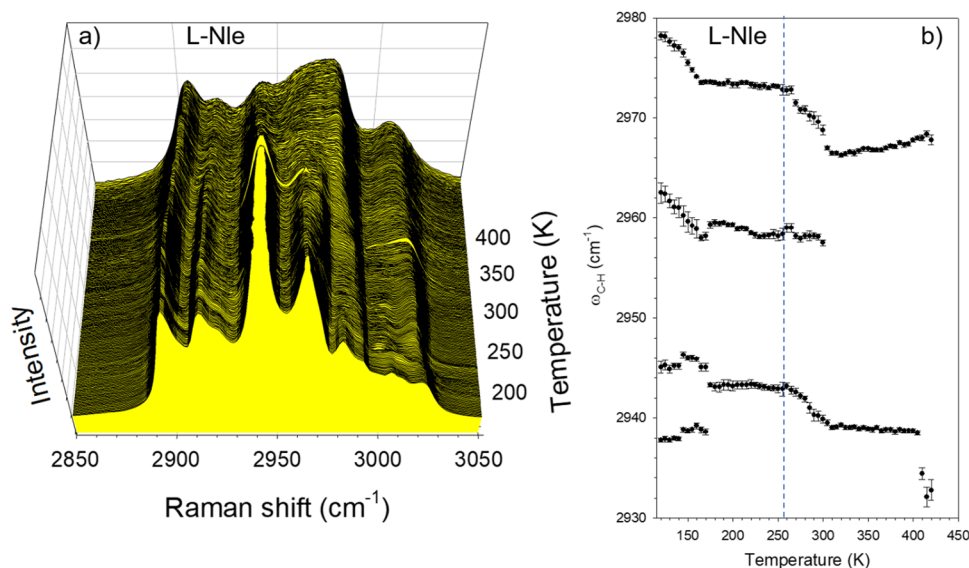


Fig. 7 Analysis of C–H stretching vibrations; temperature dependence of (a) the C–H stretching spectrum; (b) frequency of Raman bands which exhibit strong shifts.



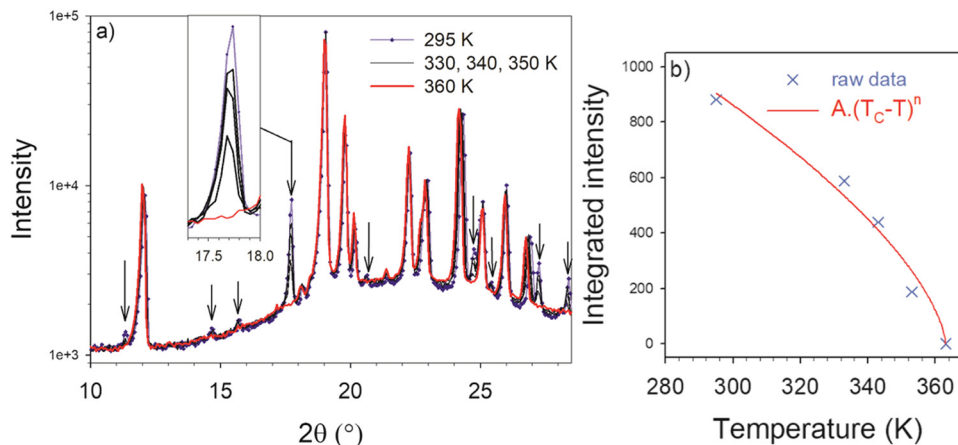


Fig. 8 Temperature dependence of the XRPD pattern of LEU. (a) XRPD patterns were plotted at temperatures at which data were collected, with a logarithm Y-scale for better highlighting reflections vanishing around 360 K (localized by arrows), and the inset shows the temperature dependence of the most intense of these reflections. (b) Temperature dependence of the integrated intensity of the most intense reflection vanishing at 360 K plotted in the inset of the XRPD patterns. The line corresponds to the fitting procedure with the function $A \cdot (T_C - T)^n$ with $T_C = 360$ K, converging towards the parameters: $A = 60 \pm 15$ and $n = 0.61 \pm 0.09$ ($R = 0.99$).

(Table S1, ESI[†]). Intriguingly, all the satellite reflections are correctly indexed using the unit cell parameters of the average structure of the INC phase, also determined in several studies performed at room temperature since 1976,^{14–16} without consideration of the existence of a modulation. Despite the absence of numerous reflections at T_C , no structural and symmetry changes can be determined from X-ray powder data. However, the vanishing of numerous weakly intense X-ray reflections supports the interpretation of the extended transformation as an INC–N phase transition. Powder diffraction data only provide information on a simple correspondence between $\|\vec{Q}_{hkl}\|$ and X-ray reflections, while the determination of the incommensurability parameter corresponding to the localization of satellites with respect to Bragg peaks requires information on \vec{Q}_{hkl} vectors, *i.e.* single crystal X-ray data. Additionally, given that the incommensurability is related to disordered CH_3 orientations and H atoms are not directly detectable by X-ray diffraction, it will be difficult to correctly determine the incommensurability parameter from X-ray powder diffraction data (Fig. 8a).

5. Consideration of both L-LEU and L-Nle studies

The existence of a normal – incommensurate phase transition both in L-leucine, revealed in the present study, and in the linear isomer (L-Nle)²² can provide information on the origin of the incommensurability. An exponential behavior of the quasi-elastic intensity was observed in the same temperature range for both compounds, identified as corresponding to the thermal activation of CH_3 rotations from the analysis of C–H stretching vibrations. This temperature range corresponds to the softening of lattice modes, but only the soft mode in L-LEU directly induces lattice instability leading to incommensurability. However, incommensurability in L-Nle occurs at significantly lower temperatures,

because of a higher degree of disorder observed by comparing Fig. 1 and 2, which could be inherent to the side-chain flexibility. It is likely that the linear molecular conformation of L-Nle induces higher side-chain flexibility than in L-LEU. This can be corroborated by the study of L-met (isosteric to L-Nle) which has revealed low-frequency Raman spectra distinctive of highly disordered state without detection of phonon peaks. In the high temperature range (> 350 K), both amino acids with linear side chains (L-Nle and L-met) exhibit lattice instabilities associated with incomplete lattice mode softening which are driven by a strong anharmonicity of CH_3 rotations leading to the partial loss of periodicity. Indeed, the low-frequency Raman spectrum resembles the VDOS of an amorphous state without detection of lattice mode while Bragg peaks remain detectable.²² This apparent contradiction issued from two different structural probes was previously observed in the rotator phase of caffeine³³ and in the metastable phase of ibuprofen.³⁴ In these cases, the molecules or molecular moieties are dynamically disordered, while the periodicity of molecular mass centers or most of the atoms within the molecule is preserved. In this context, disordering processes associated with broad endothermic features and accompanied by complete or incomplete lattice mode softening observed in several hydrophobic amino acids suggest that lattice instabilities generated by a dynamical disorder of CH_3 groups or by freezing of CH_3 rotations into disordered orientations leading to different kinds of periodicity loss could be general situations in this material family in various temperature ranges.

Conclusions

This study first reveals the incommensurability in L-leucine, an essential amino acid which is widely used as an excipient in inhaled powder formulations prepared by spray-drying, and present in a large variety of peptides and proteins throughout nature. This incommensurability is revealed *via* the observation



of a soft mode which exhibits the typical temperature dependence of the amplitudon and *via* the observation of very weakly intense X-ray reflections vanishing at 360 K, interpreted as satellite reflections. It was shown that the incommensurability was induced by the freezing of thermally-activated hydrophobic side-chain motions leading to a distribution of CH₃ orientations. In the next stage, the indexing of satellite lines will be performed from X-ray data collected in single crystals. Additionally, molecular dynamics simulation will be performed to confirm the involvement of CH₃ groups in lattice instabilities.

Additionally, consideration of results obtained on L-LEU and L-Nle and other hydrophobic amino acids from diffraction,^{22,30} thermodynamic^{12,35} and vibrational^{30,35} investigations suggests that ordering/disordering processes of terminal side-chain groups accompanied with lattice mode softening could be a general phenomenon in this class of materials. This type of phase transition often called displacive phase transition could be considered as a common character of this class of materials which have important and numerous applications in the area of the life sciences. Indeed, CH₃ reorientations can be at the origin of phase transformations in spray-dried formulations inducing protein destabilization. Hydrophobic acids are also widely used as co-formers in co-amorphous formulations. Their stability can be impacted by rotations of methyl groups. Hydrophobic amino acids are recognized to serve as a building block in protein structure. The thermal activation of CH₃ rotations could be the source of protein denaturation.

Conflicts of interest

There are no conflicts to declare.

References

- 1 M. Donovan, Y. Yimer, J. Pfaendtner, E. Backus, M. Bonn and T. Weidner, *J. Am. Chem. Soc.*, 2016, **138**, 5226–5229.
- 2 W. Doster, S. Cusack and W. Petry, *Nature*, 1989, **337**, 754–756.
- 3 H. Frauenfelder and B. McMahon, *Proc. Natl. Acad. Sci. U. S. A.*, 1998, **95**, 4795–4797.
- 4 K. Henzler-Wildman, M. Lei, V. Thai, S. Kerns, M. Karplus and D. Kern, *Nature*, 2007, **450**, 913–915.
- 5 H. Frauenfelder, S. Sligar and P. Wolynes, *Science*, 1991, **254**, 1598–1603.
- 6 J. Lewandowski, M. Halse, M. Blackledge and L. Emsley, *Science*, 2015, **348**, 578–581.
- 7 M. T. Cicerone and J. F. Douglas, *Soft Matter*, 2012, **8**, 2983–2991.
- 8 L. Chen, T. Okuda, X.-Y. Lu and H.-K. Chan, *Adv. Drug Delivery Rev.*, 2016, **100**, 102–115.
- 9 S. Mangal, F. Meiser, G. Tan, T. Gengenbach, J. Denman, M. Rowles, I. Larson and D. Morton, *Eur. J. Pharm. Biopharm.*, 2015, **94**, 160–169.
- 10 J. Yu, H. K. Chan, T. Gengenbach and J. Denman, *Eur. J. Pharm. Biopharm.*, 2017, **119**, 222–234.
- 11 P. Façanha Filho, X. Jiao, P. Freire, J. Lima Jr., A. dos Santos, P. Henry, F. Yokaichiya, E. Kremner and H. Bordallo, *Phys. Chem. Chem. Phys.*, 2011, **13**, 6576–6583.
- 12 A. Grunenberg, D. Bougeard and B. Schrader, *Thermochim. Acta*, 1984, **77**, 59–66.
- 13 P. Façanha Filho, P. Freire, K. Lima, J. Mendes Filho, F. Melo and P. Pizani, *Braz. J. Phys.*, 2008, **38**, 131–137.
- 14 C. Górbitz and B. Dalhus, *Acta Crystallogr., Sect. C: Cryst. Struct. Commun.*, 1996, **52**, 1754–1756.
- 15 K. Torii and Y. Iitaka, *Acta Crystallogr., Sect. B: Struct. Crystallogr. Cryst. Chem.*, 1971, **27**, 2237–2246.
- 16 M. Harding and R. Howieson, *Acta Crystallogr., Sect. B: Struct. Crystallogr. Cryst. Chem.*, 1976, **32**, 633–634.
- 17 L. Moroder, *J. Pept. Sci.*, 2005, **11**, 187–214.
- 18 A. Le Bail, H. Duroy and J. L. Fourquet, *Mater. Res. Bull.*, 1988, **23**, 447–452.
- 19 J. Rodriguez-Carvajal, LLB, CEA/SACLAY France 2001.
- 20 M. Coll, X. Solans, M. Font-Altaba and J. Subirana, *Acta Crystallogr., Sect. C: Cryst. Struct. Commun.*, 1986, **42**, 599–601.
- 21 R. Currat and T. Janssen, *Solid State Phys.*, 1988, **41**, 201–302.
- 22 C. H. Gorbitz, P. Karen, M. Dusek and V. Petricek, *IUCrJ*, 2016, **3**, 341–353.
- 23 Y. Guinet, L. Paccou, F. Danede and A. Hedoux, *J. Chem. Phys.*, 2022, **156**, 034501.
- 24 T. Atake, K. Nomoto, B. Chaudhuri and H. Chihara, *J. Chem. Thermodyn.*, 1983, **15**, 339–350.
- 25 J. Axe, M. Iizumi and G. Shirane, *Phys. Rev. B: Condens. Matter Mater. Phys.*, 1980, **22**, 3408.
- 26 H. Cailleau and F. Moussa, *Solid State Commun.*, 1980, **33**, 407–411.
- 27 J. F. Ryan and J. F. Scott, *Solid State Commun.*, 1974, **14**, 5–9.
- 28 S. Aubry and R. Pick, *J. Phys.*, 1971, **32**, 657–670.
- 29 A. Hédoux, L. Paccou and Y. Guinet, *J. Chem. Phys.*, 2014, **140**, 225102–225107.
- 30 J. Fischer, J. Lima, P. Freire, F. Melo, R. Havenith, J. Filho, R. Broer, J. Eckert and H. Bordallo, *Biophys. Chem.*, 2013, **180–181**, 76–85.
- 31 A. Hédoux, Y. Guinet, L. Paccou, P. Derollez and F. Danede, *J. Chem. Phys.*, 2013, **138**, 214506–214514.
- 32 L. Bernard, R. Currat, P. Delamoye, C. Zeyen, S. Hubert and R. de Kouchkovsky, *J. Phys. C: Solid State Phys.*, 1983, **16**, 433–456.
- 33 A. Hédoux, A.-A. Decroix, Y. Guinet, L. Paccou, P. Derollez and M. Descamps, *J. Phys. Chem. B*, 2011, **115**, 5746–5753.
- 34 A. Hédoux, Y. Guinet, P. Derollez, E. Dudognon and N. Correia, *Int. J. Pharm.*, 2011, **421**, 45–52.
- 35 J. Lima Jr., P. Freire, F. Melo, J. Filho, J. Fischer, R. Havenith, R. Broer and H. Bordallo, *Vib. Spectrosc.*, 2013, **65**, 132–141.

